

# Normalized Ambiguity Function Characteristics of OFDM, OTFS, AFDM, and CP-AFDM for ISAC

Hyeon Seok Rou<sup>✉</sup> and Giuseppe Thadeu Freitas de Abreu<sup>✉</sup>

*Constructor University, Bremen, Germany*

[hrou, gabreu]@constructor.university

**Abstract**—This paper presents a unified and system-agnostic analysis of the ambiguity function (AF) characteristics of four representative multicarrier waveforms, orthogonal frequency division multiplexing (OFDM), orthogonal time frequency space (OTFS), affine frequency division multiplexing (AFDM), and chirp-permuted AFDM (CP-AFDM), which are considered as key candidates for enabling integrated sensing and communications (ISAC) in future sixth generation (6G) networks. The AF of each waveform is obtained directly from its discrete-time definition and enhanced via ideal fractional interpolation, enabling precise characterization of its continuous-time delay-Doppler response. Two signaling modes are examined: a communication-oriented case with random information symbols suitable only for monostatic scenarios, and a sensing-oriented case with fixed unimodular symbols suitable for general multi-static scenarios. Furthermore, the AFs and the ambiguity metrics including the 3dB mainlobe width, peak-to-sidelobe ratio (PSLR), and integrated sidelobe ratio (ISLR), are evaluated in normalized delay-Doppler units, enabling direct translation to any physical system configuration defined by bandwidth, sampling frequency, or symbol duration, while ensuring straightforward and consistent comparison across waveforms. The results establish a consistent benchmark for comparing waveform sensing capabilities in ISAC design, consolidating known behaviors: OFDM exhibits excellent delay resolution and sidelobe behavior but poor Doppler response, whereas advanced waveforms achieve improved balance between delay and Doppler resolution with varying sidelobe characteristics. The simulation code of the smooth AFs, is openly shared to promote reproducibility and support future ISAC waveform research.

**Index Terms**—Ambiguity function, OFDM, OTFS, AFDM, CP-AFDM, delay-Doppler analysis, ISAC.

## I. INTRODUCTION

Future wireless networks are envisioned to unify communication and sensing functionalities within a single radio framework, enabling the simultaneous transmission of information and perception of the surrounding environment using a common waveform, hardware platform, and signal processing chain [1], [2]. This emerging paradigm, popularly known as integrated sensing and communications (ISAC), is one of the foundational pillars in the outlined sixth generation (6G) system definitions and requirements [3], [4].

Radar-centric ISAC approaches, which employ waveforms originally optimized for radar operation, such as frequency modulated continuous wave (FMCW), have naturally been investigated for this by embedding information into such waveforms while preserving the sensing capacity [5], [6]. However, they are constrained by their limited compatibility with existing communication standards, and often fail to meet the high data rate requirements of 6G [7].

Given these limitations, communication-centric ISAC approaches, have emerged as natural candidates for seamless integration, owing to their inherently high spectral efficiency and communications performance, compatibility with existing standards, and flexibility in waveform design [8], [9].

Among such waveforms, orthogonal frequency division multiplexing (OFDM) serves as a natural baseline, being the dominant modulation scheme in current wireless systems, in which many ISAC studies have been conducted [10], [11], highlighting its excellent delay resolution (target range) and sidelobe behavior [12], but severe limitations in Doppler resolution (target velocity). Alternatively, several advanced waveforms proposed for 6G, such as orthogonal time frequency space (OTFS) [13], [14], affine frequency division multiplexing (AFDM) [15], [16], and chirp-permuted AFDM (CP-AFDM) [17] exhibit inherently strong delay-Doppler localization, thereby implying highly attractive properties for sensing applications, particularly in the velocity estimation.

This motivates a unified and systematic comparison of waveform characteristics and sensing performance, for which we leverage the ambiguity function (AF): an intrinsic property of the transmit waveform independent of the propagation channel and system configuration, which directly reflects its range-velocity resolution and sidelobe behavior through metrics such as the mainlobe width, peak-to-sidelobe ratio (PSLR), and integrated sidelobe ratio (ISLR) [18], [19].

While the AF of individual waveforms has been investigated in many prior studies [20]–[22], these analyses have largely been conducted in isolation and lack a common framework for consistent comparison across both the delay and Doppler domains in high definition analogous to the true continuous-time behavior. Therefore, we harmonize the analysis across multiple candidate waveforms by establishing a physical system-agnostic discrete-time AF evaluation framework that employs normalized delay and Doppler coordinates, enabling simple translation to any practical system configuration, given its physical bandwidth, sampling frequency, or symbol duration.

Furthermore, to approximate the true continuous behavior, the AF is refined through optimal interpolation in delay and oversampling in Doppler, yielding smooth, high-resolution representations suitable for both visualization and quantitative metric assessment. Finally, two signaling modes are considered for comparison across all waveforms: a general ISAC mode with random information symbols, and a sensing-focused mode using deterministic unimodular symbols.

## II. SYSTEM MODEL

Consider a block of  $N$  complex information symbols  $\mathbf{x} \triangleq [x_0, x_1, \dots, x_{N-1}]^T \in \mathcal{X}^{N \times 1}$  drawn from a normalized  $M$ -ary constellation  $\mathcal{X} \subset \mathbb{C}$  with cardinality  $M$ , i.e.,  $M$ -QAM constellation. The encoding of the symbol vector  $\mathbf{x}$  into a discrete-time transmit signal  $\mathbf{s} \triangleq [s_0, s_1, \dots, s_{N-1}]^T \in \mathbb{C}^{N \times 1}$  is performed by a unitary linear modulator  $\mathbf{M} \in \mathbb{C}^{N \times N}$ . In other words, the discrete-time transmit signal vector  $\mathbf{s} \in \mathbb{C}^{N \times 1}$  is given by

$$\mathbf{s} \triangleq \mathbf{M}\mathbf{x} \in \mathbb{C}^{N \times 1}. \quad (1)$$

In light of the above, we consider four representative waveforms, namely OFDM, OTFS, AFDM, and CP-AFDM, whose respective modulation matrices  $\mathbf{M}^{\text{OFDM}}$ ,  $\mathbf{M}^{\text{OTFS}}$ ,  $\mathbf{M}^{\text{AFDM}}$ , and  $\mathbf{M}^{\text{CP-AFDM}}$  are based on the normalized  $N$ -point discrete Fourier transform (DFT) matrix  $\mathbf{F}_N \in \mathbb{C}^{N \times N}$ , whose  $(i, j)$ -th entry is given by  $[\mathbf{F}_N]_{i,n} = \frac{1}{\sqrt{N}} e^{-j2\pi \frac{in}{N}}$ . The resulting baseband transmit signals and the respective modulator structure for the four waveforms are summarized below.

### A. Orthogonal Frequency-Division Multiplexing (OFDM)

For conventional OFDM, the data symbols are mapped directly onto orthogonal subcarriers through the inverse discrete Fourier transform (IDFT), i.e.,  $\mathbf{M}^{\text{OFDM}} = \mathbf{F}_N^H$ , yielding the transmit signal

$$\mathbf{s}^{\text{OFDM}} = \mathbf{F}_N^H \mathbf{x} \in \mathbb{C}^{N \times 1}. \quad (2)$$

### B. Orthogonal Time-Frequency Space Modulation (OTFS)

The OTFS waveform is designed to provide robustness against doubly-dispersive channels by utilizing the delay-Doppler domain for information symbol placement, and have been shown to provide significant performance gains in high-mobility scenarios [13], [14]. Therefore, the information symbols are directly placed on the two-dimensional delay-Doppler grid  $\mathbf{X} \in \mathcal{X}^{K \times L}$ , with  $N = LK$ , which undergoes a two-dimensional inverse symplectic finite Fourier transform (ISFFT) and a Heisenberg transform (HT) to yield the discrete-time transmit signal. Assuming rectangular pulse shaping, the discrete-time OTFS transmit signal can be expressed as

$$\mathbf{s}^{\text{OTFS}} = \text{vec}\left(\mathbf{F}_K^H (\mathbf{F}_K \mathbf{X} \mathbf{F}_L^H)\right) = (\mathbf{F}_L^H \otimes \mathbf{I}_K) \mathbf{x} \in \mathbb{C}^{N \times 1}, \quad (3)$$

where  $\text{vec}(\cdot)$  denotes the vectorization operator and  $\otimes$  is the Kronecker product, and therefore  $\mathbf{M}^{\text{OTFS}} = (\mathbf{F}_L^H \otimes \mathbf{I}_K)$ .

### C. Affine Frequency-Division Multiplexing (AFDM)

On the other hand, the AFDM was proposed also to provide robustness against doubly-dispersive channels, by exploiting chirp-based subcarriers, and has been shown to guarantee full diversity in doubly-dispersive channels and therefore excellent performance in high-mobility scenarios [16], [23].

The AFDM waveform generalizes OFDM by extending the pure-tone subcarriers into a chirp-based subcarrier, spreading the symbols in the time-frequency domain. The modulation is concisely achieved through the inverse discrete affine Fourier transform (IDAFT), with two tunable chirp parameters  $c_1, c_2 \in$

$\mathbb{R}$ , which control the chirp rates. Given the above, the discrete-time AFDM transmit signal is given by

$$\mathbf{s}^{\text{AFDM}} = \boldsymbol{\Lambda}_{c_1}^H \mathbf{F}_N^H \boldsymbol{\Lambda}_{c_2}^H \mathbf{x} \in \mathbb{C}^{N \times 1}, \quad (4)$$

with  $\mathbf{M}^{\text{AFDM}} = \boldsymbol{\Lambda}_{c_1}^H \mathbf{F}_N^H \boldsymbol{\Lambda}_{c_2}^H$ , and  $\boldsymbol{\Lambda}_{c_i} = \text{diag}(\boldsymbol{\lambda}_{c_i})$  are the diagonal chirp matrices with chirp sequences

$$\boldsymbol{\lambda}_{c_i} = [e^{-j2\pi c_i(0)^2}, \dots, e^{-j2\pi c_i(N-1)^2}]^T \in \mathbb{C}^{N \times 1}, \quad (5)$$

for both  $c_1$  and  $c_2$ .

### D. Chirp-Permuted AFDM (CP-AFDM)

Recently, the CP-AFDM waveform was proposed to extend the AFDM by permuting the second chirp sequence  $\boldsymbol{\lambda}_{c_2}$  prior to modulation, thereby introducing an additional design degree of freedom to be utilized for additional functionalities, such as index modulation (IM) [24] or physical layer security [25], while retaining the beneficial delay-Doppler characteristics of the conventional AFDM [17].

Let  $\boldsymbol{\Pi}_i \in \mathbb{C}^{N \times N}$  be a permutation matrix corresponding to index  $i \in \{1, \dots, N!\}$ , where the permutation index  $i$  follows the lexicographic order of all possible permutations of length  $N$ . Then, by permuting the chirp sequence of the second diagonal chirp matrix as

$$\boldsymbol{\Lambda}_{c_2,i} = \text{diag}(\boldsymbol{\Pi}_i \boldsymbol{\lambda}_{c_2}) \in \mathbb{C}^{N \times N}, \quad (6)$$

the resulting discrete-time signal of the chirp-permuted AFDM with order  $i$  is simply given by

$$\mathbf{s}^{\text{CP-AFDM},i} = \boldsymbol{\Lambda}_{c_1}^H \mathbf{F}_N^H \boldsymbol{\Lambda}_{c_2,i}^H \mathbf{x} \in \mathbb{C}^{N \times 1}, \quad (7)$$

It should be noted that the modulator matrix  $\mathbf{M}^{\text{CP-AFDM},i} = \boldsymbol{\Lambda}_{c_1}^H \mathbf{F}_N^H \boldsymbol{\Lambda}_{c_2,i}^H$ , chirp-permuted inverse discrete affine Fourier transform (CP-IDAFT), remains unitary for all permutation order  $i \in \{1, \dots, N!\}$ .

## III. AMBIGUITY FUNCTION ANALYSIS

Given the above discrete-time transmit signal models of the four candidate waveforms, we now present a unified framework for directly evaluating their AF characteristics in the normalized delay-Doppler domain, enabling direct comparison and translation to arbitrary system parameters.

The AF is a fundamental descriptor of a signal's joint delay-Doppler resolution, and hence a key analytical tool for ISAC waveform design and evaluation, especially for non-radar-optimized waveforms. For a continuous-time baseband waveform  $s(t)$ , it is defined as

$$A(\tau, \nu) = \int_{-\infty}^{\infty} s(t) s^*(t - \tau) e^{-j2\pi\nu t} dt, \quad (8)$$

which measures the correlation between  $s(t)$  and a version of itself shifted in time and frequency. The mainlobe of  $|A(\tau, \nu)|$  determines the achievable delay and Doppler resolution, while sidelobes quantify potential ambiguities or interference among multiple reflections, directly affecting sensing accuracy and false detection rates.

In this work, the discrete-time AF is computed directly from the finite-length transmit vector  $\mathbf{s}$ , as described in the previous

section, whose time samples are assumed to have sampling period  $T_s = 1/f_s$ , with sampling frequency  $f_s$ . Then, the discrete AF is expressed as

$$A[\ell, k] = \sum_{n=0}^{N-1} s[n] s^*[n - \ell] e^{-j2\pi f \frac{n}{N}}, \quad (9)$$

where  $\ell$  and  $f$  denote the integer delay and Doppler indices, respectively, yielding the exact finite-sum realization of (8).

Here, normalized variables can be defined as

$$\tau_{\text{norm}} = \frac{\ell}{N}, \quad \nu_{\text{norm}} = \frac{f}{f_s}, \quad (10)$$

so that  $A(\tau_{\text{norm}}, \nu_{\text{norm}})$  is independent of sampling rate or bandwidth. In practice,  $\tau_{\text{norm}} \in [-1, 1]$  spans the full unambiguous delay range for a signal of length  $N$ , while  $\nu_{\text{norm}} \in [-0.5, 0.5]$  corresponds to the Nyquist-limited Doppler interval (cycles per sample), fully representing the centrally meaningful region without aliasing. This normalized region fully captures the intrinsic delay-Doppler characteristics of each waveform, independent of specific system parameters, and can be directly mapped to the corresponding physical quantities (time delay in seconds and Doppler shift in hertz) using

$$\tau_{\text{phys}} = \tau_{\text{norm}} T = \ell T_s, \quad \nu_{\text{phys}} = \nu_{\text{norm}} \frac{1}{T_s}, \quad (11)$$

where  $T = NT_s$  denotes the total symbol duration of the discrete block.

On top of this, to achieve smooth, high-resolution AF surfaces, both delay and Doppler axes are refined through oversampling and interpolation. In the time domain, the discrete signal is reconstructed by an ideal sinc interpolation via the sampling theorem

$$s_{\text{interp}}[t] = \sum_{n=0}^{N-1} s[n] \text{sinc}\left(\frac{t-n}{T_s}\right), \quad (12)$$

which enables the evaluation of the AF at fractional delay values with resolution  $\Delta\tau = T_s/O_\tau$ , where  $O_\tau$  is the delay oversampling factor.

For numerical implementation, however, the infinite sinc kernel is truncated and windowed to yield a practical windowed-sinc interpolation of finite support  $2L_h$  samples:

$$s_{\text{interp}}(t) \approx \sum_{n=n_0-L_h}^{n_0+L_h} s[n] w[n - n_0] \text{sinc}\left(\frac{t-nT_s}{T_s}\right), \quad (13)$$

where  $w[\cdot]$  is a smooth tapering window (e.g., Hann or Kaiser) that mitigates truncation-induced sidelobes.

Similarly, the Doppler dimension is likewise densified by evaluating (9) on a dense frequency grid  $\nu \in [-\nu_{\text{max}}, +\nu_{\text{max}}]$  with resolution  $\Delta\nu = 1/(O_\nu N)$ , where  $O_\nu$  is the Doppler oversampling factor. This continuous, oversampled representation provides a numerically stable and theoretically accurate approximation of (8), which enables a high-definition comparison of the waveform AFs, and precise extraction of key ambiguity metrics in the discrete domain.

Furthermore, while the AF is trivially in two dimensions, one-dimensional AF cross-sections are often more interpretable and relevant for practical sensing applications, as they directly reflect the waveform's resolution and ambiguity characteristics in either delay or Doppler. Namely, the zero-Doppler cut  $A_\tau[\ell] = A[\ell, 0]$ , which reflects delay resolution, and the zero-delay cut  $A_\nu[k] = A[0, k]$ , which reflects Doppler resolution. Both are obtained from the energy-normalized AF (i.e., normalized to unit peak) after interpolation, and are evaluated within the aforementioned normalized regions ( $\tau_{\text{norm}} \in [-1, 1], \nu_{\text{norm}} \in [-0.5, 0.5]$ ), ensuring complete coverage of the waveform's unambiguous sensing characteristics.

From the normalized ambiguity function cuts in zero-delay and zero-Doppler, three quantitative measures are derived to characterize the waveform behavior in delay and Doppler, respectively. This enables a comprehensive assessment of the waveform's sensing capabilities in both range and velocity estimation, which are critical for ISAC applications, rather than qualitatively comparing the AFs of different waveforms.

The first is the *3 dB mainlobe width*, which defines the half-power region surrounding the AF peak on either axis (delay or Doppler), and is computed as the width between the two points  $\xi_\pm$  where the AF magnitude drops to  $\frac{1}{\sqrt{2}}$  of its peak value, i.e.,

$$|A(\xi_\pm)| = \frac{1}{\sqrt{2}}, \quad \Delta\xi_{\text{norm}} = \xi_+ - \xi_-, \quad (14)$$

where  $\xi$  denotes either the normalized delay ( $\tau_{\text{norm}}$ ) or Doppler ( $\nu_{\text{norm}}$ ) variable.

Note that the width is measured in terms of the normalized delay or Doppler units of eq. (8), such that it can be translated to the practical resolutions given the system parameters using eq. (11). Trivially, a narrower mainlobe implies finer range or velocity resolution.

To characterize the sidelobe behavior of each waveform, the peak-to-sidelobe ratio (PSLR) and integrated sidelobe ratio (ISLR) metrics are evaluated, quantifying respectively the peak and total sidelobe energy relative to the mainlobe. While these measures are conventionally computed over the entire two-dimensional AF surface, in our article, we evaluate them specifically along the *zero-Doppler* and *zero-delay* cuts, only. This one-dimensional formulation isolates the waveform behavior in the pure delay and Doppler domains, offering a clearer and more interpretable assessment of range- and velocity-related ambiguity characteristics that are intuitively most relevant for ISAC analysis.

Given the above, the PSLR, commonly measured in dB scale, along a given 1D cut in the  $\xi$ -domain (where  $\xi \in \{\tau, \nu\}$ ) is defined as

$$\text{PSLR}_\xi = 20 \log_{10} \left( \frac{\max_{\xi \in \text{sidelobes}} |A(\xi)|}{\max_\xi |A(\xi)|} \right), \quad (15)$$

which describes the relative height of the highest sidelobe to the central mainlobe peak, such that lower (more negative) values correspond to stronger sidelobe suppression and lower false-target probability.

On the other hand, the ISLR in dB scale, is defined as the ratio between the total energy in the sidelobes to the energy in the mainlobe, given by

$$\text{ISLR}_\xi = 10 \log_{10} \left( \frac{\sum_{\xi \in \text{sidelobes}} |A(\xi)|^2}{\sum_{\xi \in \text{mainlobe}} |A(\xi)|^2} \right), \quad (16)$$

where a smaller ISLR indicates greater energy concentration within the mainlobe and reduced energy leakage.

In the ISAC context, these normalized metrics collectively capture the fundamental sensing properties of a waveform: the 3 dB width determines range or velocity resolution, the PSLR measures resistance to false detections, and the ISLR reflects the overall energy leakage. Therefore, in practice, these metrics well describe the waveform's ability and efficiency to accurately estimate target range and velocity in the presence of multiple reflections, which is critical for 6G scenarios.

#### IV. SIMULATION RESULTS AND ANALYSIS

Based on the above waveform formulations and the AF analysis framework, we now present and discuss the numerical results comparing the AF characteristics of the four candidate waveforms: OFDM, OTFS, AFDM, and CP-AFDM. Owing to the normalized formulation, these results are fully system-agnostic and can be directly translated to any practical system configuration, enabling fair and consistent comparison across different waveform types. Furthermore, the smoothing and interpolation techniques yield high-resolution AF surfaces and cuts, enabling precise extraction of the key ambiguity metrics, independent of the underlying discrete sample size  $N$ .<sup>1</sup>

Two signaling scenarios are considered in the analysis. The first corresponds to the general random-symbol case, where the transmitted symbols are streams of information, are drawn from a complex modulation alphabet. This setting reflects practical ISAC operation, in which the waveform must simultaneously convey information and perform sensing. Here, the ambiguity function represents the average behavior under typical data transmission, offering a realistic assessment of sensing performance during concurrent communication.

However, the inherent randomness of the transmitted symbols influences the correlation structure of the waveform and consequently alters the AF shape and associated metrics. Furthermore, this mode is only valid for sensors (i.e., receivers) that have perfect knowledge of the transmitted symbols in order to perform the matched correlator to obtain the radar responses, which is not always the case in practical ISAC scenarios, unless a monostatic configuration is assumed.

Therefore, to assume a more general multi-static case, and also to reveal these underlying core characteristics of the waveform structure independent of data randomness, a second unimodular or *sensing-only* scenario is also examined, in which all transmitted symbols are set to unity. As an example, such sensing-only operation can be realized in practice by allocating specific time-frequency resources or pilot blocks for dedicated sensing transmissions within an ISAC frame.

<sup>1</sup>To promote reproducibility and support future ISAC waveform research, the MATLAB simulation scripts for the fractionally-interpolated ambiguity functions are publicly available at our repository: [online].

#### A. AF Under Random Symbols

Figures 1 and 2 illustrate the corresponding AFs of the four candidate waveforms, with random-symbol averages over  $R = 1 \times 10^4$  independent realizations of normalized 16-QAM symbols. For the CP-AFDM, the permutation index  $i \in \{1, \dots, N!\}$  was also randomized for each realization, to reflect the average behavior across all possible permutations, although different permutations can yield slightly different instantaneous AF shapes. Block sizes of  $N = 144$  symbols for all waveforms ( $K \times L = 12 \times 12$  for OTFS), with interpolation factors  $O_\tau = 4$  and  $O_\nu = 4$  for delay and Doppler, with  $L_h = 4$  have been utilized for the numerical simulations.

As can be seen, the AF characteristics are similar across all waveforms, in both the delay and Doppler domains, with the mainlobes being very sharp with low sidelobes, with OFDM exhibiting a comparative lower sidelob in the delay domain than other waveforms, as also reported in [12]. Thanks to the randomness of the symbols, which effectively decorrelates the waveform and suppresses sidelobes, this indicates good delay-Doppler resolution. However, as mentioned, this case is only valid for receivers with perfect knowledge of the transmitted symbols (i.e., monostatic ISAC), which is not always practical in general ISAC scenarios.

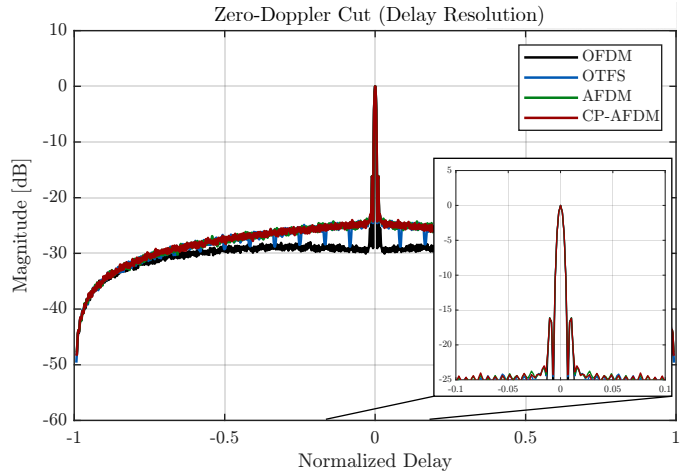


Fig. 1: Average zero-Doppler AF cuts for random 16-QAM signaling.

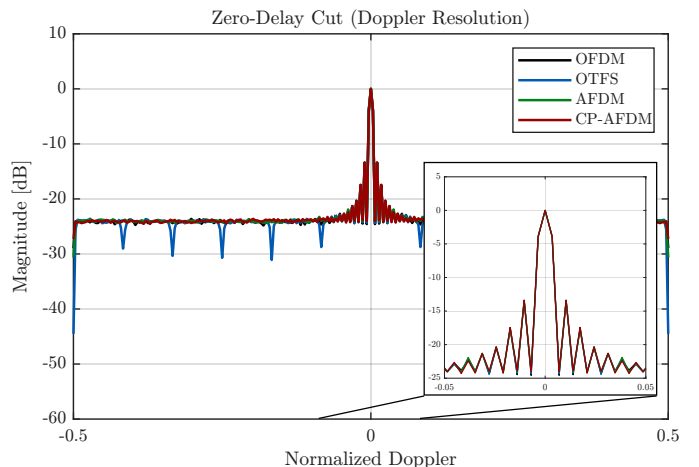


Fig. 2: Average zero-delay AF cuts for random 16-QAM signaling.

TABLE I: Normalized AF metrics extracted from 1D cuts (Figs. 3 and 4), for the unit symbol case ( $N = 144$ ,  $K = L = 12$ ,  $O_\tau = 4$ ,  $O_\nu = 4$ ,  $L_h = 4$ ).

Waveform	$\Delta\tau_{3dB}$	$\Delta\nu_{3dB}$	$PSLR_\tau$	$ISLR_\tau$	$PSLR_\nu$	$ISLR_\nu$
OFDM	0.0058	1.8021	-16.0975	-313.0712	-14.8007	-183.6956
OTFS	0.0493	0.0740	-43.8373	-13.0694	-51.4935	-6.8425
AFDM	0.0058	0.0056	-6.0206	-13.4633	-0.7274	-9.4944
CP-AFDM	0.0059	0.0058	-16.0286	-14.8963	0.1036	2.6158

### B. AF Under Unimodular Symbols

Figures 3 and 4 illustrate the normalized zero-Doppler and zero-delay AF cuts for the case where all transmitted symbols are set to unity. This configuration isolates the intrinsic ambiguity properties of each waveform, independent of symbol randomness, and is relevant for radar-like or multi-static ISAC scenarios in which deterministic signals are employed.

In this setting, distinct differences emerge across the four waveforms. From the zero-Doppler cuts in Fig. 3, OFDM, AFDM, and CP-AFDM exhibit sharply concentrated mainlobes with varying sidelobe characteristics, whereas OTFS presents a moderately broader mainlobe. OFDM achieves the lowest sidelobe levels, consistent with its well-known delay resolution properties, while AFDM exhibits higher sidelobe peaks around  $\pm 0.5$  normalized delay, which are effectively mitigated in CP-AFDM variant.

Conversely, in the zero-delay cuts of Fig. 4, the limited Doppler resolution of OFDM becomes apparent, with a nearly flat mainlobe. In contrast, both AFDM and CP-AFDM achieve distinct and narrow Doppler mainlobes, while OTFS exhibits a wider but still well-defined response. AFDM demonstrates the cleanest Doppler-domain behavior with a monotonically decaying sidelobe envelope, followed by CP-AFDM and OTFS, which display comparatively stronger sidelobes.

It is important to note that the aforementioned behaviors generally hold across all valid parameterizations of the respective waveforms, of course with OFDM lacking any adjustable parameter, but OTFS on the delay-Doppler lattice dimensions ( $K, L$ ), AFDM on the chirp parameters  $(c_1, c_2)$ , and CP-AFDM on the chirp parameters  $(c_1, c_2)$  and additionally on the permutation index  $i$ . This highlights the robustness of the observed ambiguity characteristics and highlights the flexibility of these advanced waveforms in adapting to different configurations while preserving their fundamental delay-Doppler properties.

Finally, to quantitatively support these observations and provide a consistent benchmark of each waveform's intrinsic sensing characteristics, Table I summarizes the extracted normalized AF metrics for the unimodular case, including the 3 dB mainlobe widths, PSLR, and ISLR. All quantities are expressed in normalized delay-Doppler units, enabling direct translation to physical parameters such as time delay and Doppler frequency. Accordingly, the presented results remain fully system-agnostic and can be readily mapped to any practical configuration of bandwidth, sampling rate, or symbol duration. It should be noted that although OFDM appears to exhibit excellent PSLR and ISLR in the Doppler domain as well, this effect arises from its excessively wide mainlobe,

which makes the sidelobes negligible in relative magnitude. Therefore, this is not directly meaningful, as the waveform inherently suffers from extremely poor Doppler resolution.

### V. CONCLUSION

We presented a unified, system-agnostic framework to compare the ambiguity functions of OFDM, OTFS, AFDM, and CP-AFDM under both random-symbol and unimodular signaling. By evaluating the discrete-time AF, applying windowed-sinc delay interpolation and dense Doppler sampling for higher definition, and reporting normalized cut-based metrics (3 dB width, PSLR, ISLR), our results enable fair, portable comparisons across systems. The methodology provides a concise reference for ISAC waveform selection, highlighting and comparatively illustrating the inherent delay-Doppler characteristics of each candidate waveform.

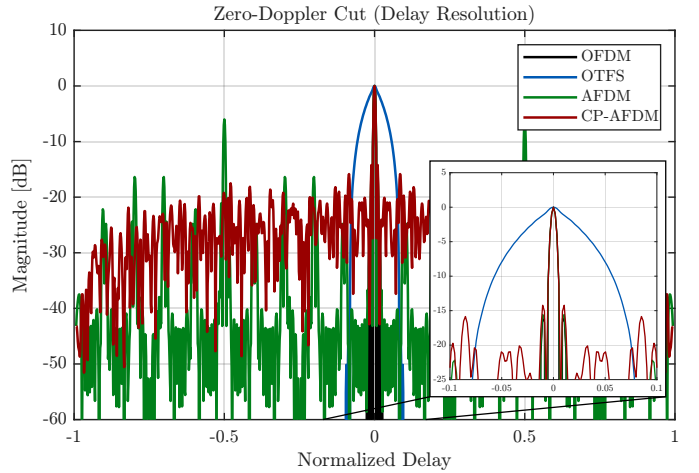


Fig. 3: Zero-Doppler AF cuts for unit symbol signaling.

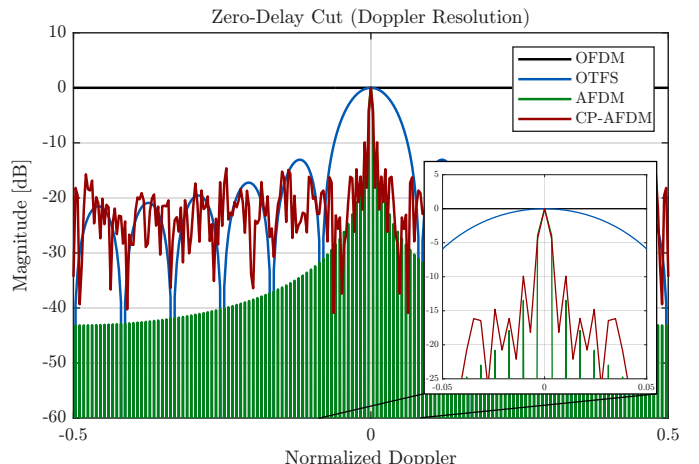


Fig. 4: Zero-delay AF cuts for unit symbol signaling.

## REFERENCES

- [1] M. Z. Chowdhury, M. Shahjalal, S. Ahmed, and Y. M. Jang, “6G wireless communication systems: Applications, requirements, technologies, challenges, and research directions,” *IEEE Open Journal of the Communications Society*, vol. 1, pp. 957–975, 2020.
- [2] C.-X. Wang, X. You, X. Gao, X. Zhu, Z. Li, C. Zhang, H. Wang, Y. Huang, Y. Chen, H. Haas, J. S. Thompson, E. G. Larsson, M. D. Renzo, W. Tong, P. Zhu, X. Shen, H. V. Poor, and L. Hanzo, “On the Road to 6G: Visions, Requirements, Key Technologies, and Testbeds,” *IEEE Communications Surveys & Tutorials*, vol. 25, no. 2, pp. 905–974, 2023.
- [3] A. Kaushik, R. Singh, S. Dayarathna, R. Senanayake, M. Di Renzo, M. Dajer, H. Ji, Y. Kim, V. Sciancalepore, A. Zappone, and W. Shin, “Toward integrated sensing and communications for 6G: Key enabling technologies, standardization, and challenges,” *IEEE Communications Standards Magazine*, vol. 8, no. 2, pp. 52–59, 2024.
- [4] F. Liu, Y. Cui, C. Masouros, J. Xu, T. X. Han, Y. C. Eldar, and S. Buzzi, “Integrated sensing and communications: Toward dual-functional wireless networks for 6G and beyond,” *IEEE Journal on Selected Areas in Communications*, vol. 40, no. 6, pp. 1728–1767, 2022.
- [5] M. Temiz, N. J. Peters, C. Horne, M. A. Ritchie, and C. Masouros, “Radar-centric ISAC through index modulation: Over-the-air experimentation and trade-offs,” in *2023 IEEE Radar Conference (RadarConf23)*, 2023, pp. 1–6.
- [6] D. Ma, N. Shlezinger, T. Huang, Y. Shavit, M. Namer, Y. Liu, and Y. C. Eldar, “Spatial modulation for joint radar-communications systems: Design, analysis, and hardware prototype,” *IEEE Transactions on Vehicular Technology*, vol. 70, no. 3, pp. 2283–2298, 2021.
- [7] J. A. Zhang, F. Liu, C. Masouros, R. W. Heath, Z. Feng, L. Zheng, and A. Petropulu, “An overview of signal processing techniques for joint communication and radar sensing,” *IEEE Journal of Selected Topics in Signal Processing*, vol. 15, no. 6, pp. 1295–1315, 2021.
- [8] V. Koivunen, M. F. Keskin, H. Wymeersch, M. Valkama, and N. González-Prelcic, “Multicarrier ISAC: Advances in waveform design, signal processing, and learning under nonidealities [Special issue on signal processing for the integrated sensing and communications revolution],” *IEEE Signal Processing Magazine*, vol. 41, no. 5, pp. 17–30, 2024.
- [9] H. S. Rou, G. T. F. de Abreu, J. Choi, D. González G., M. Kountouris, Y. L. Guan, and O. Gonsa, “From orthogonal time-frequency space to affine frequency-division multiplexing: A comparative study of next-generation waveforms for integrated sensing and communications in doubly dispersive channels [Special issue on signal processing for the integrated sensing and communications revolution],” *IEEE Signal Processing Magazine*, vol. 41, no. 5, pp. 71–86, 2024.
- [10] K. M. Braun, “OFDM radar algorithms in mobile communication networks,” Ph.D. dissertation, Karlsruhe, Karlsruher Institut für Technologie (KIT), Diss., 2014, 2014.
- [11] Q. Dai, Y. Zeng, H. Wang, C. You, C. Zhou, H. Cheng, X. Xu, S. Jin, A. L. Swindlehurst, Y. C. Eldar *et al.*, “A tutorial on MIMO-OFDM ISAC: From far-field to near-field,” *arXiv preprint arXiv:2504.19091*, 2025.
- [12] F. Liu, Y. Zhang, Y. Xiong, S. Li, W. Yuan, F. Gao, S. Jin, and G. Caire, “CP-OFDM achieves the lowest average ranging sidelobe under QAM/PSK constellations,” *IEEE Transactions on Information Theory*, 2025.
- [13] R. Hadani, S. Rakib, M. Tsatsanis, A. Monk, A. J. Goldsmith, A. F. Molisch, and R. Calderbank, “Orthogonal time frequency space modulation,” in *2017 IEEE wireless communications and networking conference (WCNC)*. IEEE, 2017, pp. 1–6.
- [14] Z. Wei, W. Yuan, S. Li, J. Yuan, G. Bharatula, R. Hadani, and L. Hanzo, “Orthogonal time-frequency space modulation: A promising next-generation waveform,” *IEEE wireless communications*, vol. 28, no. 4, pp. 136–144, 2021.
- [15] A. Bemani, N. Ksairi, and M. Kountouris, “Affine frequency division multiplexing for next generation wireless communications,” *IEEE Transactions on Wireless Communications*, vol. 22, no. 11, pp. 8214–8229, 2023.
- [16] H. S. Rou, K. R. R. Ranasinghe, V. Savaux, G. T. F. de Abreu, D. González G., and C. Masouros, “Affine Frequency Division Multiplexing (AFDM) for 6G: Properties, Features, and Challenges,” *arXiv preprint arXiv:2507.21704*, 2025.
- [17] H. S. Rou and G. T. F. de Abreu, “Chirp-permuted AFDM: A new degree of freedom for next-generation versatile waveform design,” *arXiv preprint arXiv:2507.20825*, 2025.
- [18] M. A. Richards, J. A. Scheer, and W. A. Holm, *Principles of modern radar: basic principles*. IET, 2010.
- [19] J. Li and P. Stoica, *MIMO radar signal processing*. John Wiley & Sons, 2008.
- [20] H. Yin, Y. Tang, Y. Ni, Z. Wang, G. Chen, J. Xiong, K. Yang, M. Kountouris, Y. L. Guan, and Y. Zeng, “Ambiguity function analysis of AFDM signals for integrated sensing and communications,” *IEEE Journal on Selected Areas in Communications*, 2025.
- [21] B. Wang, X. Wei, X. Li, and Y. Zhou, “The optimal tradeoff between PAPR and ambiguity functions for generalized OFDM waveform set in ISAC systems,” *arXiv preprint arXiv:2503.21239*, 2025.
- [22] R. Chong, S. Li, F. Liu, Y. Xiong, W. Yuan, G. Caire, and M. Matthaiou, “Delay-doppler ISAC: Ambiguity function analysis via Zak-OTFS modulation,” in *IEEE Global Communications Conference (GLOBECOM) 2025*.
- [23] A. Bemani, N. Ksairi, and M. Kountouris, “Affine frequency division multiplexing for next generation wireless communications,” *IEEE Transactions on Wireless Communications*, vol. 22, no. 11, pp. 8214–8229, 2023.
- [24] H. S. Rou, K. Yukiyoshi, T. Mikuriya, G. T. F. de Abreu, and N. Ishikawa, “AFDM chirp-permutation-index modulation with quantum-accelerated codebook design,” in *2024 58th Asilomar Conference on Signals, Systems, and Computers*, 2024, pp. 817–821.
- [25] H. S. Rou and G. T. F. de Abreu, “Chirp-permuted AFDM for quantum-resilient physical-layer secure communications,” *IEEE Wireless Communications Letters*, 2025.